Clinical Ophthalmology

Dovepress
open access to scientific and medical research

Open Access Full Text Article

ORIGINAL RESEARCH

# Analysis of Peripapillary Intrachoroidal Cavitation and Myopic Peripapillary Distortions in Polar Regions by Optical Coherence Tomography

Adèle Ehongo[1], Noélie Bacq[1], Nacima Kisma[1], Artemise Dugauquier[1], Yassir Alaoui Mhammedi[1], Kevin Coppens[2], Françoise Bremer[1], Karelle Leroy[3]

[1]Ophthalmology Department, Erasmus Hospital, Brussels, 1070, Belgium; [2]Statistician, Cosma Consulting, Enghien 7850, Belgium; [3]Histology Department, Erasmus Campus, CP 620, Université Libre de Bruxelles, Brussels, 1070, Belgium

Correspondence: Adèle Ehongo, Ophthalmology Department, Erasmus Hospital, Route de Lennik 808, Brussels, 1070, Belgium, Tel +3225553114, Fax +3225556737, Email adele.ehongo@erasme.ulb.ac.be

**Purpose:** To compare the peripapillary polar characteristics in eyes combining peripapillary staphyloma and gamma peripapillary atrophy according to whether peripapillary intrachoroidal cavitation (PICC) was present or absent (combination-group).

**Patients and methods:** This prospective non-interventional cross-sectional study included 667 eyes of 334 subjects. From the polar peripapillary regions to the opening of Bruch's membrane, the following elements and their topographic relationships were analyzed using optical coherence tomography sections: configuration of the posterior curvature of the choroid, visibility of the subarachnoid space (SAS), and suprachoroidal detachment (SCD). Chi-squared and Fisher exact tests were used for statistical analysis.

**Results:** The protrusion of the posterior choroidal wall, with anterior elevation on either side, observed in both groups progressed and transformed into a wedge-shaped deformity on the side of gamma peripapillary atrophy. This wedge configuration was significantly more frequent in PICC-group than in combination-group ($p = 0.004$ and $p < 0.001$) for the upper and lower poles, respectively. SAS was more frequently observed in PICC-group than in combination-group ($p = 0.002$ and $p < 0.001$) for the upper and lower poles, respectively. SCD was detected exclusively in PICC-group ($p < 0.001$, both poles). The wedge-shaped configuration and the SCD were aligned antero-posteriorly with the SAS.

**Conclusion:** We confirmed that PICC is an SCD. We observed its constant alignment with the SAS. We suggest that the tensile forces of the optic nerve sheaths during adduction promote the collapse of the scleral flange onto the SAS, leading to PICC. Further studies are warranted to confirm this hypothesis.

**Keywords:** peripapillary intrachoroidal cavitation, suprachoroidal detachment, gamma peripapillary atrophy, staphyloma, subarachnoid space, myopic complications

## Introduction

Recently, we observed that peripapillary intrachoroidal cavitation (PICC), a complication found in highly myopic eyes[1,2] occurs exclusively in eyes combining gamma peripapillary atrophy (γPPA) and a peripapillary staphyloma (PPS) (unpublished), suggesting structural peculiarities of the peripapillary region when these anomalies coexist. However, only 22.75% of eyes with this coexistence also exhibit PICC. Therefore, among the eyes with this combination, the question arises of the difference between those with (PICC-group) and those without (combination-group) PICC.

The positional relationship of (peri)papillary structures is known to be influenced by myopic changes,[3] including tilted disc (TD) in which Optical Coherence Tomography (OCT) studies have shown that structures are posteriorly positioned on γPPA side.[4–6] The deep polar peripapillary regions, located at the intersection of zones with and without γPPA, are thus transition areas where contiguous structures are in different antero-posterior planes.

PPS is mainly characterized on OCT by choroidal thickening restricted around the optic nerve (ON),[7] along a posterior scleral protrusion,[7–9] with on either side, choroidal thinning along the anterior scleral elevation.[7,10]

Received: 29 May 2022
Accepted: 4 August 2022
Published: 13 August 2022

When a TD and a PPS coexist, their specificities could thus interfere and lead, among others, to a PICC. The exact factors involved in the formation of a PICC from these two entities remain unclear.

Recent biomechanical studies have shown that the ON sheaths exert high magnitude tensile forces on their scleral insertions during eye movements, leading consistently to significant (peri)papillary strains[11–19] with backward and forward displacements of, respectively, temporal and nasal structures, following adduction.

Of note, in high myopia, the scleral flange (sclera between ON's margin and dura mater) is lengthened and extremely thin.[20,21] The retrobulbar subarachnoid space (SAS) behind it can thus be observed using OCT.[22] As the mechanical stress mentioned above is exacerbated in myopic eyes,[11,18] the landmarks around the SAS could be useful for biomechanical analysis of the (peri)papillary area in these eyes.

Given these considerations, we aimed to study by OCT, the configuration of the posterior curvature of the choroid from the peripapillary polar regions to Bruch's membrane's opening (BMO) in the presence or absence of PICC. We sought to verify that PICC is a suprachoroidal detachment (SCD) and finally, we looked for the topographic landmarks that surround it, to understand the potential mechanisms involved in its genesis.

## Materials and Methods

This was an observational, cross-sectional, monocentric study approved by the Ethics Committee of Erasmus Hospital (Brussels, Belgium), (reference P2019/281). The study complied with the tenets of the Declaration of Helsinki and written informed consent was acquired from all participants.

### Inclusion Population

Subjects without a history of ocular trauma or posterior segment surgery, and aged 18 years or older, were recruited over 12 months. Participants were approached during their routine visit to our service and through various information channels.

The refractive error (RE) and axial length (AL) thresholds were set according to the International Classification of Diseases.[23] A minimum number of 100 highly myopic eyes (diopter $\leq -6$ or AL $\geq$ 26 mm) were set based on the prevalence of PICC.[1,2] At least 50 eyes were sought for each of the other three refractive groups.[23] Operated eyes with an unknown preoperative RE were excluded unless AL was ≥26 mm, classifying them as highly myopic.

### General and Ocular Data

Age, gender, and ocular laterality were recorded for each subject. A comprehensive ophthalmic examination including AL measurement with IOL Master® (Carl Zeiss Meditec, Jena, Germany) was conducted in both eyes of the subjects. Color fundus pictures were taken using a VISUCAM® non-mydriatic camera (PRO NM Carl Zeiss Meditec, Jena, Germany) and Spectral Domain OCT imaging using Spectralis® HRA-OCT (Heidelberg Engineering GmbH, Heidelberg Germany) was performed.

### OCT Imaging Acquisition

Radial OCT acquisitions were made using the commercialized *Glaucoma Premium Edition* module of the Spectralis®. Linear (horizontal and vertical) scans, centered on ON head were performed. For TD, linear sections intercepting both the γPPA and the preseptal ON were also made. A rectangular acquisition of at least 15° × 25° was imaged, each section resulting from the summation of at least 60 confocal frames. In the presence of a PPS, its limits determined as much as possible the rectangle of acquisition. A case was also imaged by Swept source OCT, using Topcon Dri OCT Triton® with radial scans acquisition.

### OCT Analysis Procedure

One out of 4 of the 48 spokes provided by the OCT module, corresponding to the twelve clock-hourly positions, was analyzed on the radial sections. Linear sections were examined from the peripapillary area toward the BMO.

Each variable was analyzed independently by two readers (AE, YAM). The results, recorded in the patient's file were confronted by a third investigator (NB). In case of doubt on the interpretation of data on a slice, a refinement was made

by using those on both sides. If the ambiguity persisted, the option *undefined* was noted in the file. In the event of disagreement, the data was reviewed independently by the investigators. If the disagreement persisted, the data was also marked as *undefined* in the file.

## OCT Data - Sample Population

PICC,[24–26] PPS[7–10] and γPPA[5,6,27] were identified on radial and confirmed on linear sections according to their reported diagnostic criteria in OCT. The γPPA was the surrogate marker for TD.[5,6,27] Based on OCT criteria, eyes were sorted into five groups according to the presence or absence of PICC, PPS and TD. Three groups were formed each with eyes endowed with one of these entities: one group with eyes combining PPS and TD, and the last group with eyes presenting none of the entity.

Eyes with *undefined* data for the diagnosis of these three entities and therefore not allowing them to be classified in one or the other group were excluded.

Using linear OCT sections, the following other data were then analyzed.

The curvature of the posterior wall of the choroid was analyzed from the peripapillary zone of the upper and lower poles toward the BMO.

The interface between the posterior wall of the choroid and the preseptal ON overlaid by the Bruch's membrane was analyzed in the peripapillary zone. An OCT section through the ON head shows that from the BMO to the lamina cribrosa, the neural canal widens (Figure 1A). Thus, each linear OCT section located in the area extending from the BMO

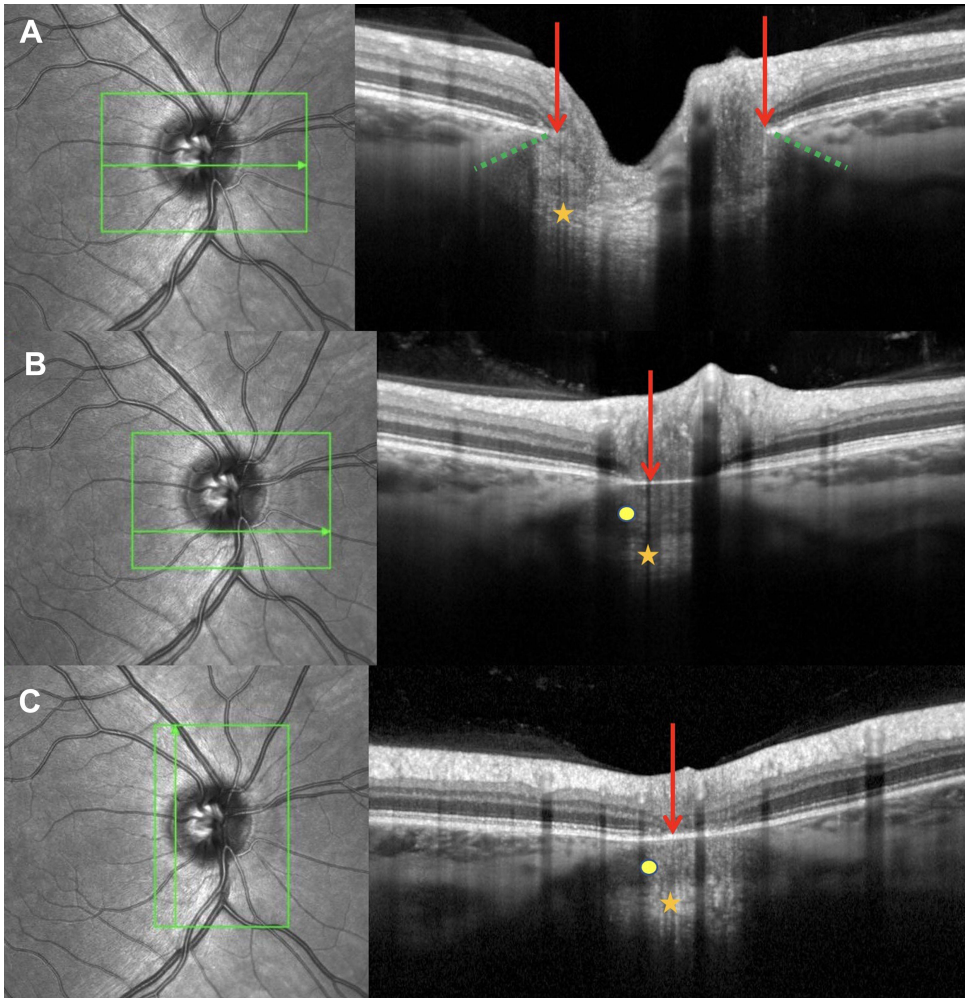


**Figure 1** OCT sections illustrating the "embedded" optic nerve (EON). (**A**–**C**) Bruch's membrane (BM): red arrows. Lamina cribrosa (LC): orange star. (**A**) Section through ON showing widening of neural canal (dashed green line) from BM to LC. (**B**) Horizontal and (**C**) vertical slices as displayed in infrared images. The EON (Yellow dot) is between BM and LC.

to the outer limit of the lamina cribrosa intercepts the prelaminar ON behind the Bruch's membrane (Figure 1B and C). In this article, we refer to this part of the ON as the "embedded" ON. The discontinuity of the border tissue of the embedded ON was defined as the interruption or the absence of its reflectance on the OCT, observed in at least two different slices.

The diagnosis of an SCD was based on the detection of a hypo-reflective space between the sclera and the Bruch's membrane, with linear reflectivity separating it anteriorly from the presumed initial choroid (Spaide).[26]

SAS was searched for at the upper and lower peripapillary areas of the poles, and the configuration of the posterior choroidal wall or the scleral flange in front of it was recorded.

All *undefined* data were excluded from statistical analysis to limit potential bias. Of note, to preserve sample size, all eyes were retained at this stage as the undefined element was not the same from eye to eye.

## Statistical Analysis

The data listed above were reported on an Excel spreadsheet for statistical analysis, using Excel. Eyes with PICC were compared both to the rest of the sample population and to the combination-group. The student's *t*-test was used for continuous variables and the Chi-squared test or the Fisher's exact test for the categorical ones. A p-value of less than 5% was considered statistically significant.

# Results

## Characteristics of the Sample Population

Six hundred sixty-seven eyes from 334 subjects, including 203 women (60.8%) were recruited, of which 229 highly and 438 non-highly myopic. The mean age was 49.7 ± 18.0 years (range: 18–91 years). Forty-nine eyes (7.3%) were excluded because assessment of at least one of the entities (PICC, PPS or TD) was questionable. Of the 618 remaining eyes, 40 (6.5%) had a PICC and 136 (22%) combined PPS and TD without PICC. We found a TD without PPS in 198 eyes (32%), 16 eyes (2.6%) presented PPS without TD and 228 eyes (36.9%) had none of these entities. The demographic and ocular characteristics of the sample population are summarized in Table 1.

No significant difference was found in gender repartition between subjects with and without PICC (p = 0.90). The other characteristics were significantly different between the two groups (Table 1).

There was no significant difference between PICC and combination groups for any feature (Table 1).

## Posterior Choroidal Wall Configuration

From poles to ON, in all groups, the serial OCT sections showed a convexity of the posterior wall of the choroid (Figure 2A–D, lines 1) that disappeared, revealing the embedded ON behind (Figure 2A-B, lines 2) before the BMO (Figure 2A and B, lines 3). In the presence of a PPS, the posterior convexity increased between anterior distortions (Figure 2C, line 2), and then disappeared, also showing the embedded ON (Figure 2C, line 3) before the BMO

**Table 1** General and Ocular Characteristics of Each Group of the Sample Population

| | PICC n = 40 | PPS+TD n = 136 | PPS n = 16 | TD n = 198 | None of these Entities n = 228 | No PICC n = 578 | *p* | *p** |
|---|---|---|---|---|---|---|---|---|
| Age (y), mean ± σ (median) | 59.6 ± 17.0 (63) | 60.3 ± 15.7 (64.5) | 62.1 ± 7.1 (62) | 43.0 ± 17.3 (40) | 46.1 ± 16.5 (47) | 48.8 ± 17.9 (51) | <0.001 | 0.80 |
| AL (mm), mean ± σ (median) | 26.7 ± 2.2 (26.2) | 26.2 ± 1.6 (26.2) | 25.2 ± 2.1 (25.6) | 25.2 ± 1.5 (25.2) | 23.7 ± 1.0 (23.5) | 24.8 ±1.7 (24.6) | <0.001 | 0.19 |
| RE (D), mean ± σ (median) | −7.4 ± 5.7 (−6.6) | −6.3 ± 4.3 (−5.9) | −4.1 ± 3.9 (−4.7) | −3.8 ± 3.7 (−3.9) | −0.3 ± 2.6 (0) | −3.0 ± 4.2 (−2.25) | <0.001 | 0.26 |
| VA (LogM), mean ± σ (median) | 0.1 ± 0.3 (0.0) | 0.0 ± 0.1 (0) | 0.0 ± 0.1 (0) | 0 ± 0.1 (0) | −0.0 ± 0.1 (0) | 0 ± 0.08 (0) | 0.008 | 0.07 |

**Notes**: p = significance of differences between PICC group and the rest of the study group. P* = significance of differences between PICC group and the combination group.
**Abbreviations**: PICC, peripapillary intrachoroidal cavitation; PPS, peripapillary staphyloma; TD, tilted disc; No PICC, the sample population without PICC; AL, axial length; RE, refractive error; VA, visual acuity.

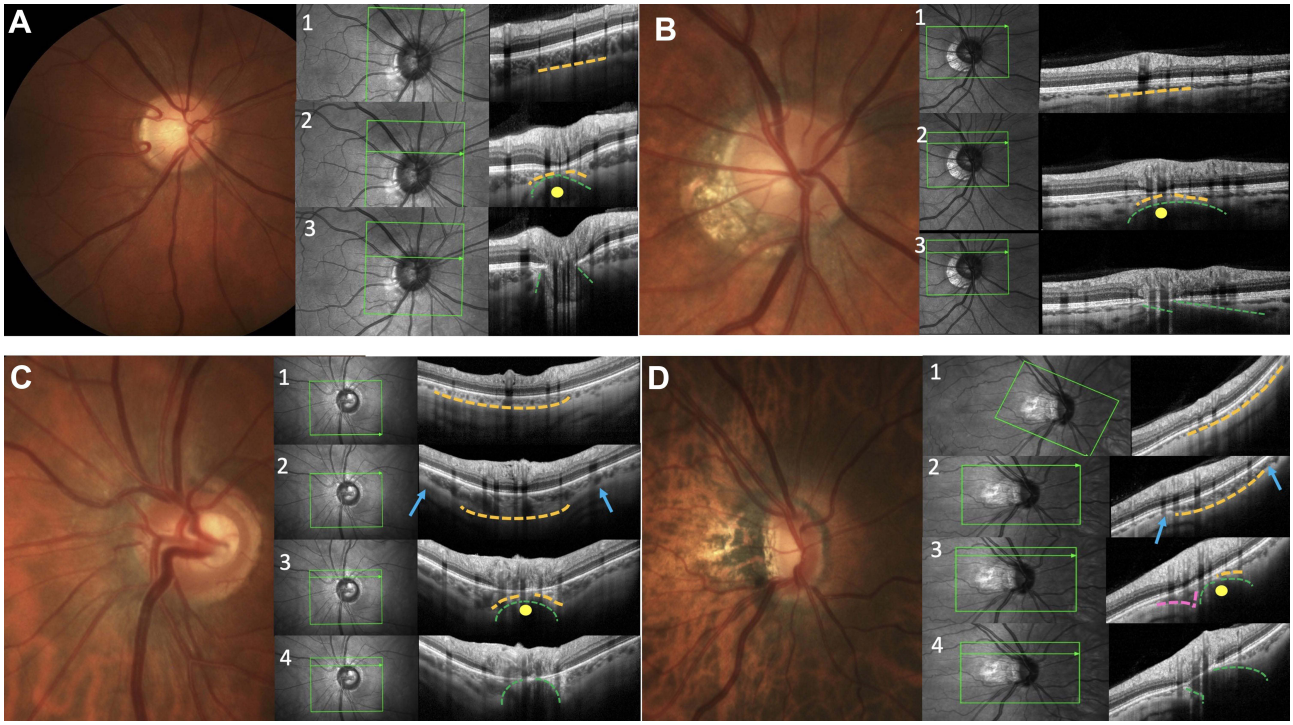


**Figure 2** Serial OCT sections disclosing the configuration of the posterior choroidal wall (PCW) in groups without peripapillary intrachoroidal cavitation. (**A–D**) LEFT: Each group's fundus image. RIGHT: OCT slice as shown in the infrared image of each line. PCW: dashed orange line. Border tissue: dashed green curve. Yellow dot: embedded optic nerve. (**A**) None of the entities. (**B**) Tilted disc. In both cases, the sequence (lines 1-2-3) is: PCW convexity-loss of it-Bruch's membrane opening (BMO). (**C**) Peripapillary staphyloma. (**D**) Combination. Lines 1–2 in both cases: Increase in PCW convexity between anterior distortions (blue arrows). Lines 3: loss of convexity for (**C**), PCW wedge deformation (dashed pink lines) for (**D**). Line 4: BMO for both.

(Figure 2C, line 4). Combination and PICC groups revealed an additional wedge-shaped configuration. The entire sequence of configurations is displayed in Figure 2D lines 1–4, and Figure 3A–H for combination and PICC respectively. The wedge configuration was significantly more frequent in the PICC-group (Table 2).

## Discontinuity of the Embedded Optic Nerve's Border Tissue

The discontinuity of the border tissue of the embedded ON (Figure 3G) was exclusively found in PICC-group: 6 and 12 eyes, respectively, at the superior and inferior poles (Table 2).

## Suprachoroidal Detachment and Subarachnoid Space

Of 40 eyes diagnosed with PICC, 3 were in the upper pole, 36 in the lower pole and the remaining eye had PICC in both poles.

Identification of SCD was questionable (mainly due to tissular disorganization) in 1 of 4 and in 9 of 37 PICCs respectively at the upper and lower poles. A total of 10 PICCs were thus classified as "undefined" according to the OCT diagnostic criteria for SCD stated above.

Thus, in the remaining sample of 30 eyes, SCD (Figure 3D–H) was unambiguously identified in 3/3 and 28/28 PICCs, respectively, at the upper and lower poles.

SAS was observed in 68 (11.8%) and 95 (16.4%) eyes of the whole population, respectively, at the upper and lower poles. It was more frequently observed in the PICC than the combination groups ($p = 0.002$) and ($p < 0.001$), respectively, for the upper and lower poles (Table 3).

Vertical and horizontal OCT slices through the (peri)papillary zone allowing the detection of SAS are shown in Figure 4A and B for combination eyes. For a PICC (Figure 4C), this is also shown in Figure 4D and E.

SAS and the wedge configuration of the posterior choroidal wall consistently shared the same anteroposterior alignment (Figure 5B and C) when identified concomitantly. Their concomitant identification was more frequent in the

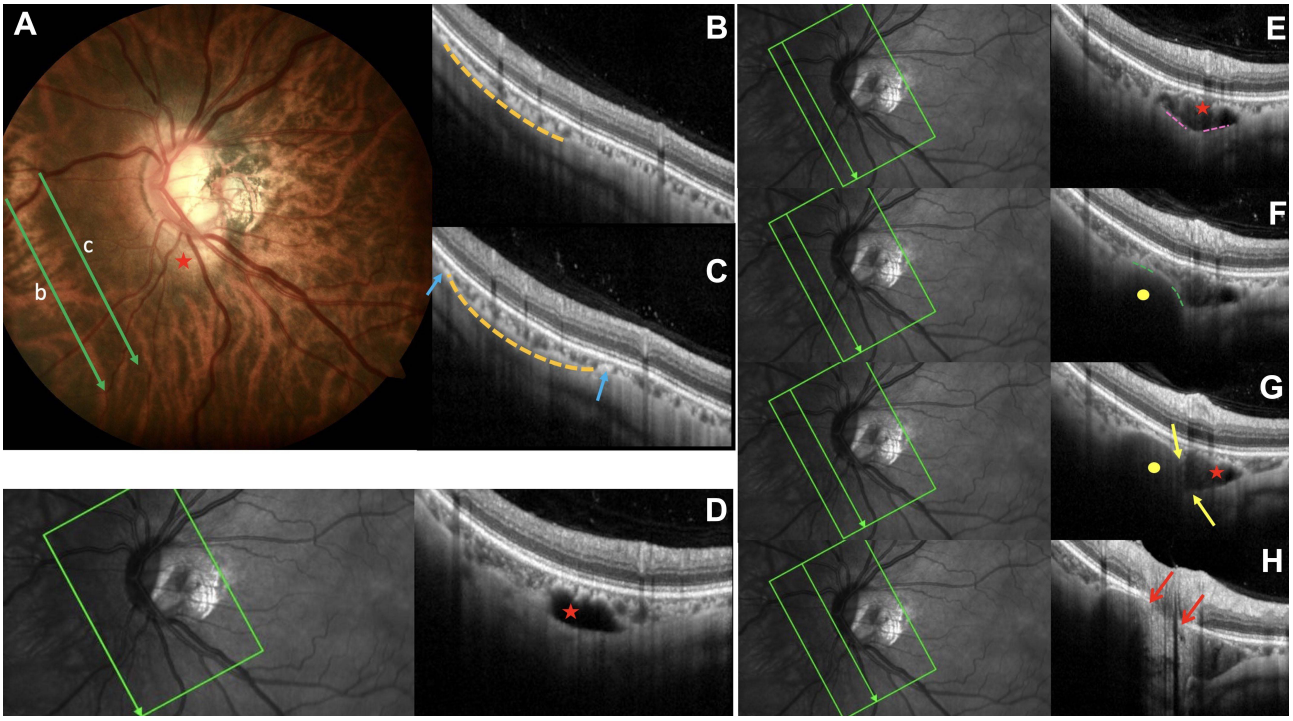


**Figure 3** Serial OCT sections disclosing the configuration of the posterior choroidal wall (PCW) in a case of peripapillary intrachoroidal cavitation (PICC). (**A**) Fundus image with PICC (red star) displaying arrows (b) and (c) for slices (**B**) and (**C**). (**B** and **C**) Increased PCW (dashed orange line) convexity between anterior distortions (blue arrows). (**D**–**H**) Slices as shown in each infrared image. (**D**) Suprachoroidal detachment (red star). (**E**) Wedge distortion of the PCW (dashed pink lines). (**F**) Continuous border tissue (BT) (dashed green lines) of the embedded optic nerve (EON) (yellow dot). (**G**) BT discontinuity (yellow arrows) between the choroidal space (red star) and the EON. (**H**) Opening of Bruch's membrane between the red arrows.

PICC-group than in the combination-group: (12 versus 8) and (19 versus 8) eyes, respectively, for upper and lower poles (Table 3).

## Evaluation of the Axial Length According to the Visibility of the SAS

Mean AL was significantly higher in the group with detected SAS than in that with undetected SAS ($p < 0.001$) regardless of pole (Table 4).

# Discussion

The increasing prevalence of myopia,[28–30] which in turn implies that a percentage of these individuals will have high myopia at some point in their lives, with the risk of retinal complications (as suggested by various studies),[28,29] has made myopia-related retinal and choroidal complications a public health issue. Although this myopia epidemic is much more severe in South and East Asian countries, there has also been an increasing prevalence of myopia among children in urban areas of countries in other continents,[29,31] hence the prediction of pathologic myopia as a major cause of visual impairment worldwide.[32]

Our results showed that AL and myopic RE were significantly higher in eyes with than those without PICC, which is consistent with previous work[33] and suggests a higher risk of related myopic retinal complications in PICC group.[28] Of note, the PICC and combination groups showed no significant difference for AL or myopic RE, which is unprecedented as these groups had never been compared head-to-head.

Our results showed significantly higher AL in the detected SAS group than that with undetected SAS, which is consistent with previous work,[34] supporting the hypothesis that myopic elongation of the eye along with thinning and lengthening of the peripapillary scleral flange[20,21] allows detection of SAS[22] using OCT. Of note, although the PICC and combination groups showed no significant difference in mean AL or RE, SAS detection was more frequent in the former group. Further studies are warranted to clarify this point which may be related to the pathogenesis of PICC.

**Table 2** Configuration of the Posterior Wall of the Choroid. Discontinuity of Embedded Optic Nerve's Border Tissue

| | | PICC n = 40 | PPS +TD n = 136 | PPS n = 16 | TD n = 198 | None of these Entities n = 228 | No PICC (n = 578) | *P* | *P** |
|---|---|---|---|---|---|---|---|---|---|
| **Loss of convexity superior pole** | Undefined (%) | 4/40 (10) | 3/136 (2.2) | / | 4/198 (2) | / | 7/578 (1.2) | | |
| | Present (%) | 36/36 (100) | 127/133 (95.5) | 15/16 (93.8) | 182/194 (93.8) | 225/228 (98.7) | 549/571 (96.1) | 0.63 Fisher | 0.34 Fisher |
| **Loss of convexity inferior pole** | Undefined (%) | 5/40 (12.5) | 3/136 (2.2) | / | 4/198 (2) | / | 7/578 (1.2) | | |
| | Present (%) | 33/35 (94.3) | 97/133 (72.9) | 14/16 (87.5) | 148/194 (76.3) | 221/228 (96.9) | 480/571 (84.1) | 0.44 $Chi^2$ | 0.7 $Chi^2$ |
| **Wedge configuration superior pole** | Undefined (%) | 4/40 (10) | 4/136 (2.9) | / | 6/198 (3) | / | 10/578 (1.7) | | |
| | Present (%) | 16/36 (44.4) | 21/132 (15.9) | 3/16 (18.8) | 7/192 (3.6) | 0/228 (0) | 31/568 (5.5) | < 0.001 Fisher | 0.04 $Chi^2$ |
| **Wedge configuration inferior pole** | Undefined (%) | 8/40 (20) | 5/136 (3.7) | / | 4/198 (2) | 1/228 (0.4) | 10/578 (1.7) | | |
| | Present (%) | 21/32 (65.6) | 11/131 (8.4) | 0/16 (0) | 2/194 (1.0) | 0/227 (0) | 13/568 (2.3) | < 0.001 Fisher | < 0.001 $Chi^2$ |
| **Discontinuity of the BT of the embedded ON superior pole** | Undefined (%) | 4/40 (10) | 3/136 (2) | / | 4/198 (2) | / | 7/578 (1.2) | | |
| | Present (%) | 6/36 (17) | 0/133 (0) | 0/16 (0) | 0/194 (0) | 0/228 (0) | 0/571 (0) | < 0.001 Fisher | < 0.001 Fisher |
| **Discontinuity of the BT of the embedded ON inferior pole** | Undefined (%) | 9/40 (22.5) | 4/136 (3) | / | 4/198 (2) | / | 8/578 (1) | | |
| | Present (%) | 12/31 (39) | 0/132 (0) | 0/16 (0) | 0/194 (0) | 0/228 (0) | 0/570 (0) | < 0.001 Fisher | < 0.001 Fisher |

**Notes**: p = significance of differences between PICC group and the rest of the study group, p*= significance of differences between PICC-group and the combination-group.
**Abbreviations**: PICC, peripapillary intrachoroidal cavitation; PPS, peripapillary staphyloma; TD, tilted disc; No PICC, the sample population without PICC; BT, border tissue; ON, optic nerve.

**Table 3** Suprachoroidal Detachment, SAS, Wedge-Shaped Choroidal Wall Deformation

| | | PICC n = 40 | PPS +TD n = 136 | PPS n = 16 | TD n = 198 | None of the Entities n = 228 | No PICC = 578 | *P* | *P** |
|---|---|---|---|---|---|---|---|---|---|
| **SCD superior pole** | Undefined (%) | 1/40 (2.5) | 3/136 (2.2) | / | 4/198 (2) | / | 7/578 (1.2) | | |
| | Present (%) | 3/39 (7.7) | 0/133 (0) | 0/16 (0) | 0/194 (0) | 0/228 (0) | 0/571 (0) | < 0.001 Fisher | < 0.001 Fisher |
| **SCD inferior pole** | Undefined (%) | 9/40 (22.5) | 3/136 (2.2) | / | 4/198 (2) | / | 7/578 (1.2) | | |
| | Present (%) | 28/31 (90.3) | 0/133 (0) | 0/16 (0) | 0/194 (0) | 0/228 (0) | 0/571 (0) | < 0.001 Fisher | < 0.001 Fisher |

(*Continued*)

**Table 3** (Continued).

| | | PICC n = 40 | PPS +TD n = 136 | PPS n = 16 | TD n = 198 | None of the Entities n = 228 | No PICC = 578 | *P* | *P** |
|---|---|---|---|---|---|---|---|---|---|
| **Wedge form superior pole** | Present (%) | 16/36 (44.4) | 21/132 (15.9) | 3/16 (18.8) | 7/192 (3.6) | 0/228 (0) | 31/568 (5.5) | < 0.001 Fisher | 0.004 $Chi^2$ |
| **Wedge form inferior pole** | Present (%) | 21/32 (65.6) | 11/131 (8.4) | 0/16 (0) | 2/194 (1.0) | 0/227 (0) | 13/568 (2.3) | < 0.001 Fisher | < 0.001 $Chi^2$ |
| **Detection of SAS, superior pole** | Undefined (%) | 7/40 (18) | 21/136 (15) | / | 15/198 (8) | / | 36/578 (6.2) | | |
| | Present (%) | 21/33 (64) | 31/115 (27) | 0/16 (0) | 16/183 (9) | 0/228 (0) | 47/542 (8.7) | < 0.001 $Chi^2$ | 0.002 $Chi^2$ |
| **Detection of SAS inferior pole** | Undefined (%) | 7/40 (18) | 18/136 (13) | / | 13/198 (7) | / | 31/578 (5.3) | | |
| | Present (%) | 27/33 (82) | 46/118 (39) | 0/16 (0) | 22/185 (12) | 0/228 (0) | 68/547 (12.4) | < 0.001 $Chi^2$ | < 0.001 $Chi^2$ |
| **Wedge/SAS alignment, superior pole** | Undefined (%) | 28/40 (70) | 128/136 (94) | / | 198/198 (100) | / | / | | |
| | Present (%) | 12/12 (100) | 8/8 (100) | / | / | / | / | / | / |
| **Wedge/SAS alignment, inferior pole** | Undefined (%) | 20/40 (50) | 128/136 (94) | / | 197/198 (99) | / | / | | |
| | Present (%) | 19/20 (95) | 8/8 (100) | / | 1/1 (100) | / | / | / | / |

**Notes**: p = significance of differences between PICC-group and the rest of the study group. p* = significance of differences between PICC-group and combination-group. Wedge/SAS alignment = co-alignment of the wedge-shaped deformity of the posterior choroidal wall with the SAS.

**Abbreviations**: PICC, peripapillary intrachoroidal cavitation; PPS, peripapillary staphyloma; TD, tilted disc; No PICC, the sample population without PICC; SCD, suprachoroidal detachment; SAS, subarachnoid space.

Regarding the posterior choroidal wall, its convexity was lost before the BMO in all the groups, but it presented specificities for some of them.

In PPS, the initial curvature of the posterior choroidal wall became more pronounced and positioned between anterior warpings of this wall. The choroid thickened along the convexity but showed a pinching at each of its edges, a hallmark of the PPS.[10] When PPS and TD coexisted, the accentuation of the posterior convexity led to a posterior wedge deformity on the side of γPPA, more frequent in the PICC-group. We thus suggest that interference between the structural features of these entities promotes wedge deformation and that PICC eyes are more exposed or sensitive to causal conditions than combination eyes. To our knowledge, this posterior wedge configuration has never been described before.

The posterior wedge deformity of choroidal wall on the γPPA side suggests cross-forces at the polar peripapillary regions. From there and considering both the biomechanical data on the ON,[11–19] and the landmarks of the scleral insertions of the ON sheaths,[20–22,35] we propose a hypothesis of the elements participating in the genesis of the PICC.

Our results confirmed (unpublished data) that at the edge of the choroidal thickening of a PICC, the choroid is thinned along the anterior warping of its posterior wall. We suggest that thinning of the choroid might result from the tangential components of the tensile force exerted by the dura on its scleral insertions. As Bruch's membrane is very strong[36] and maintains its plane, the choroid thins out at these pressure areas and repositions around them (Figure 5A). Thinning of the choroid under compression has recently been reported and supports our hypothesis.[15,37]

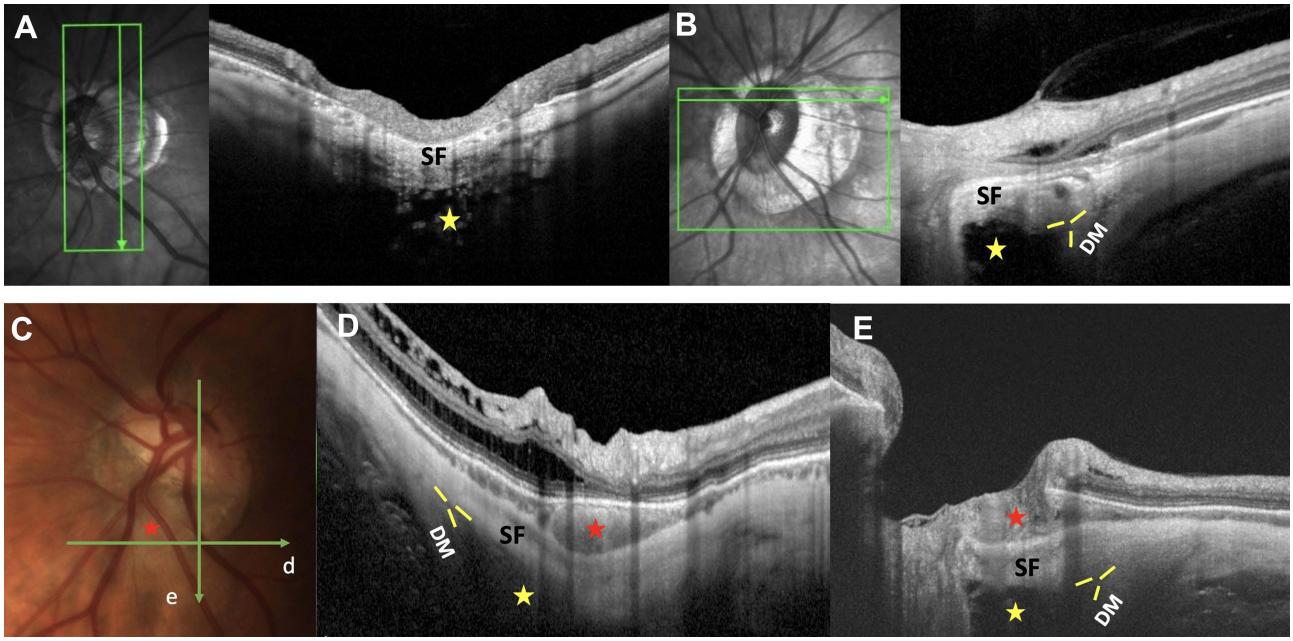


**Figure 4** Subarachnoid space visibility- Peripapillary intrachoroidal cavitation (PICC) landmarks. (**A** and **B**) Eyes without PICC. Section as displayed in each infrared image. The subarachnoid space (SAS) (yellow star) is behind the scleral flange (SF). (**B**–**E**). The three yellow lines highlight the transition zone between the SF, sclera and dura mater (DM). (**C**) Fundus image with PICC (red star) displaying arrows d and e for slices (**D**) and (**E**) respectively. SF between SAS and PICC (red star).

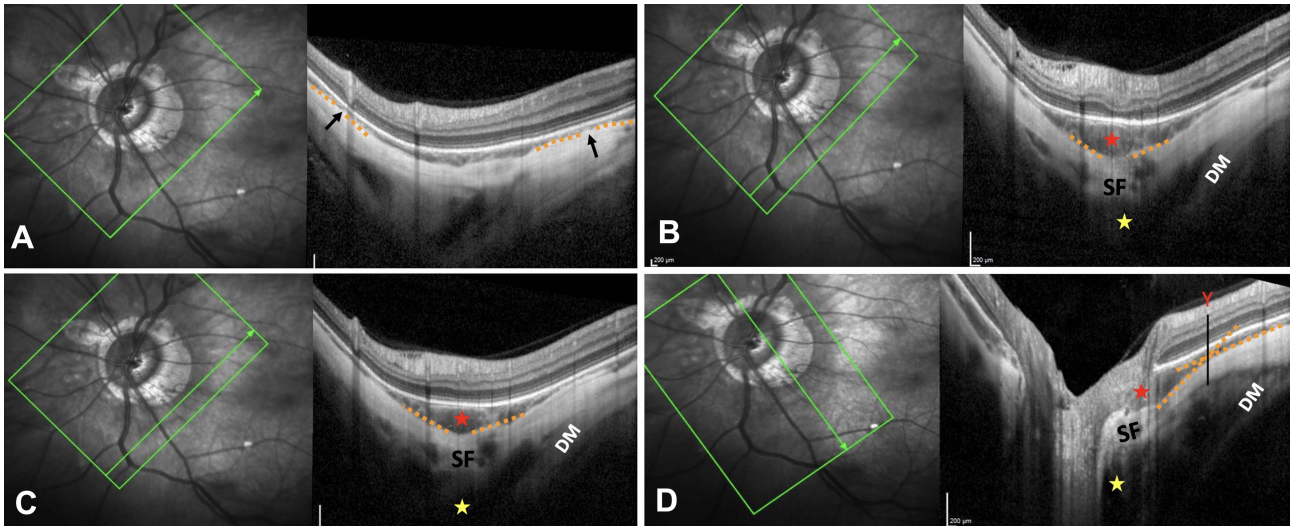


**Figure 5** Pathogenetic hypothesis of peripapillary intrachoroidal cavitation (PICC). (**A**–**D**) Sections as displayed in each infrared image. Dashed orange line: posterior choroidal wall (PCW). (**A**) The choroid is thickened between and thinned along the anterior distortions (black arrows) of the PCW. (**B**–**D**) Red star: PICC. Yellow star: subarachnoid space (SAS). Scleral flange: SF. DM: Dura mater. (**B** and **C**). Alignment of the wedge-shaped PCW (and PICC) with SAS. (**D**) The PCW distortion shows two slopes on either side of the "Y" line.

Serial OCT sections showed that the accentuation of the convexity of the choroidal wall coincided with the visualization of the dura (Figure 5B). We thus suggest that the posterior scleral deformity results from the direct posterior traction exerted by the dura on the thinned and weakened myopic structures. Spaide et al showed that in PICC, thickening of the choroid results from posterior excursion of the sclera.[26] Our results support this theory and further suggest that the driving force behind this excursion is dura traction.

Our results showed that PICC and SAS are aligned anteroposteriorly (Figure 5B and C). The detection of SAS on the OCT slices coincided with that of a second accentuation of the posterior curvature of the choroidal wall. We hypothesize

**Table 4** Distribution of the Axial Length According to the Detection of SAS

| Undefined (n) | SAS Visibility (n) | | Axial Length (mm) Mean ± σ | P (Student Test) |
|---|---|---|---|---|
| Upper Pole 43/618 | Detected | 68/575 | 26.7±1.9 | **<0.001** |
| | Undetected | 507/575 | 24.6 ± 1.6 | |
| Lower Pole 38/618 | Detected | 95/580 | 26.6±1.8 | **<0.001** |
| | Undetected | 485/580 | 24.5 ± 1.5 | |

**Note**: p = significance of differences between detected and undetected SAS.
**Abbreviation**: SAS, subarachnoid space.

that the scleral outpouching can then be divided into two components: the first, in front of the dura, and a second part, following a steeper slope and ending in front of the SAS (Figure 5D). The scleral flange, which was thinned and lengthened beforehand due to myopic changes, sags over the SAS. Moreover, recent observations reveal that the dura in adults has a bilaminar structure[38] contributing to the local difference in the level of stress it applies, its maximum tensile stiffness being in its inner layer, next to the SAS.[39]

If the posterior depression of the scleral flange is located at the intersection of the lines of force just explained, the posterior wall of the choroid deforms into a wedge, with a triangular thickening of the choroid in front of it (Figure 5B and C) and (Figure 6A).

Our results showed that the SCD is exclusively observed in the PICC. We thus confirm that the PICC is indeed an SCD as previously reported.[26] Like SAS, SCD was aligned with the accentuation of the curvature of the posterior choroidal wall. We therefore suggest that dura traction leads to SCD; Traction induces choroidal thickening as the scleral flange recedes, while Bruch's membrane maintains its plane. Subsequently, dissociation between the suprachoroid and the scleral flange occurs (Figure 6A). Cleavage rather occurs in the suprachoroid because the choriocapillaris and Bruch's membrane form a single unit.[36]

Discontinuity of the embedded ON's border tissue was exclusively found in the PICCs. To the best of our knowledge, it has never been described before. Serial OCT sections showed the embedded ON's imprint at the ON-choroid interface, suggesting a forward compression of the choroid by it (Figure 3F) and (Figure 6B–D). The embedded ON is fixed to the lamina cribrosa,

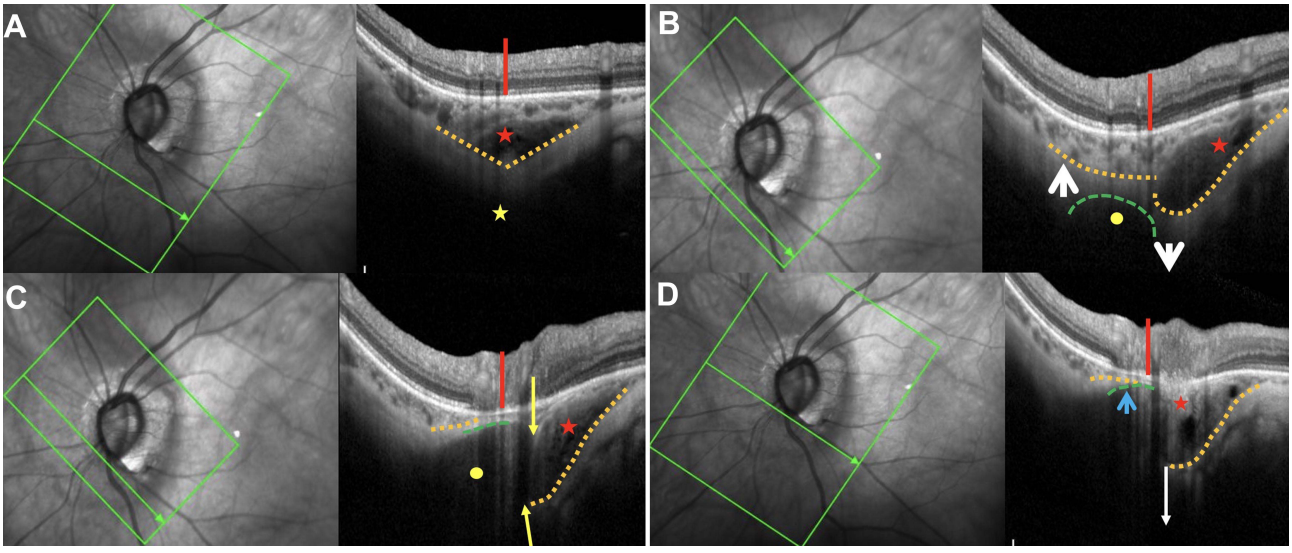


**Figure 6** Discontinuity of the border tissue (BT) of the "embedded" optic nerve (EON): pathogenetic hypothesis. (**A**–**D**) Serial peripapillary OCT slices (shown in infrared images). Bruch's membrane plane (red line) is preserved. Dashed orange line: posterior choroidal wall (PCW). Red star: peripapillary intrachoroidal cavitation (PICC). (**A**) PICC clearly appears as a suprachoroidal detachment. The wedge-shaped PCW aligns with PICC and subarachnoid space (yellow star). (**B**–**D**). Dashed green line: BT of the EON (yellow dot). (**B**) Lamina cribrosa tilting (white arrows). (**C**) BT discontinuity (yellow arrows). (**D**) Opposite stress on the BT: meningeal traction (white arrow) and tilting of the EON (blue arrow).

thus they both experience anterior nasal positioning during the adduction-induced see-saw motion. The temporal (peri) papillary structures are pulled posteriorly by the ON sheaths[13,15–17] including the border tissue, which is in continuity with the pia mater.[21,34,40] At the ON-choroid interface, the embedded ON's border tissue is thus exposed to these two stresses in opposite directions (Figure 6B), stretches, and ultimately breaks (Figure 6C and D).

PICC occurs exclusively in eyes combining a PPS and γPPA (unpublished). However, the exact origin of these two entities remains unknown. In our hypothesis, posterior dura traction increases the convexity of the posterior choroidal wall, while a tangential component of this traction squeezes the choroid at the edges of the convexity. The features of PPS could reflect an accentuation of these stresses and/or a greater tissue sensitivity to them. On the other hand, repeated see-saw motions of the (peri)papillary structures are suggested to be the cause of TD.[14,15] Both PPS and TD could then result from ON sheath tractions on the peripapillary sclera during adduction.

Thus, accentuated traction forces of the ON sheaths during adduction[11,17–19,41] promote (peri)papillary myopic complications.[4,13–15] Moreover, the dura[38] applies higher stress in its inner part, mechanically overloading[39] the lamina cribrosa which is the main site[42] of ON damage in glaucoma. This could explain some of the visual field defects found in PICC[1,43] as well as the high prevalence of glaucoma in myopic eyes.[44] Interestingly and supporting this hypothesis, strong adduction-induced strains on (peri)papillary structures have recently been demonstrated in glaucoma[19,45,46] and may therefore explain the pressure-independent component of visual field defects in glaucoma. Understanding the mechanisms favoring the appearance of visual field defects in all these entities will shed new light on their clinical management.

## Limitations - Perspectives

First, our pathogenic hypothesis implies that the tractions exerted by the dura mater on its insertion could be the cause of PICC. However, and although the confocal performance of our SD-OCT device improves the sharpness and the accuracy of the pictures, artifacts due to elongated myopic eyes limited the depth of sharpness. Thus, the dura mater and its scleral insertions were only visible in a few cases. Future studies circumventing this drawback will provide more data to confirm our hypothesis. Second, the potential impact of meningeal traction intensity and scleral resistance could not be assessed in our fully OCT-based study. Prospective biomechanical and longitudinal studies specifically designed for this purpose will shed light on these points. Third, in its intraorbital course, the ON is directed forwards, outward and downward. Its impact during adduction is therefore not limited to simple papillary rotation on the vertical axis. Future studies should thoroughly explore rotation around other axes in myopic TD.

## Conclusion

In TD associated with high myopia, there is an extension of the SAS linked to that of the scleral flange, which is also thinner. As a result, the scleral flange, weakened beforehand, undergoes significant strains, resulting in its posterior collapse and an SCD. PICC could thus be defined as a detachment of the suprachoroid in the peripapillary polar region following the recession of a thinned scleral flange, subjected to traction by the dura. It lies partly along the expanded SAS. This phenomenon is probably promoted by adduction movements. Besides, the peripapillary choroid is thickened but presents a pinching at the limit of this thickening, corresponding to the edge of the scleral tethering of the dura mater: this corresponds to the definition of a PPS.

This study shed new light on three peripapillary complications of high myopia, allowing us to establish a link between TD and PPS as critical factors for the PICC emergence, to define the PICC and to suggest a hypothesis of mechanical development of PICC.

Moreover, we describe the discontinuity of the embedded ON's border tissue, which is found exclusively in the PICC and supports the biomechanical theory of its genesis. To our knowledge, this is the first article mentioning this feature.

Further longitudinal and biomechanical prospective studies are needed to specify the role of ON movements on (peri) papillary structures in high myopia though.

## Acknowledgments

The authors thank Pr. Viviane de Maertelaere, (Emeritus and invited Professor of Biostatistics, ULB, Faculty of Medicine IRIBHM, Brussels, Belgium), for her contribution to the study design and in estimating the minimum number of highly myopic patients to include based on the prevalence of PICC.

They are also grateful to Mr. Driss Khayer, (Department of Ophthalmology, Erasmus Hospital, Brussels, Belgium) who performed most of the OCT acquisitions.

## Funding

No funding was received for this research.

## Disclosure

The authors report no conflicts of interest in this work.

## References

1. Shimada N, Ohno-Matsui K, Yoshida T, et al. Characteristics of peripapillary detachment in pathologic myopia. *Arch Ophthalmol*. 2006;124(1):46–52. doi:10.1001/archopht.124.1.46
2. You QS, Peng XY, Chen CX, Xu L, Jonas JB. Peripapillary intrachoroidal cavitations. The Beijing eye study. *PLoS One*. 2013;8(10):e78743. PMID: 24302981; PMCID: PMC3840228. doi:10.1371/journal.pone.0078743
3. Sawada Y, Araie M, Shibata H, et al. Optic disc margin anatomic features in myopic eyes with glaucoma with spectral-domain OCT. *Ophthalmology*. 2018;125(12):1886–1897. doi:10.1016/j.ophtha.2018.07.004
4. Jonas JB, Wang YX, Zhang Q, et al. Parapapillary gamma zone and axial elongation–associated optic disc rotation: the Beijing Eye Study. *Invest Ophthalmol Vis Sci*. 2016;57:396–:402. doi:10.1167/iovs.15-18263
5. Fan YY, Jonas JB, Wang YX, Chen CX, Wei WB. Horizontal and vertical optic disc rotation. The Beijing Eye Study. *PLoS One*. 2017;12(5):e0175749. doi:10.1371/journal.pone.0175749
6. Kim M, Choung HK, Lee KM, Oh S, Kim SH. Longitudinal Changes of optic nerve head and peripapillary structure during childhood myopia progression on OCT. Boramae myopia cohort study report 1. *Ophthalmology*. 2018;125(8):1215–1223. doi:10.1016/j.ophtha.2018.01.026
7. Shinohara K, Moriyama M, Shimada N, Yoshida T, Ohno-Matsui K. Characteristics of peripapillary staphylomas associated with high myopia determined by swept-source optical coherence tomography. *Am J Ophthalmol*. 2016;169:138–144. doi:10.1016/j.ajo.2016.06.033
8. Ohno-Matsui K. Proposed classification of posterior staphylomas based on analyses of eye shape by three-dimensional magnetic resonance imaging. *Ophthalmology*. 2014;121(9):1798–1809. doi:10.1016/j.ophtha.2014.03.035
9. Spaide RF. Staphyloma: part 1. In: Spaide RF, Ohno-Matsui K, Yannuzzi LA, editors. *Pathologic Myopia*. New York: Springer; 2014:167–176.
10. Tanaka N, Shinohara K, Yokoi T, et al. Posterior staphylomas and scleral curvature in highly myopic children and adolescents investigated by ultra-widefield optical coherence tomography. *PLoS One*. 2019;14(6):e0218107. PMID: 31181108; PMCID: PMC6557512. doi:10.1371/journal.pone.0218107
11. Demer JL. Optic nerve sheath as a novel mechanical load on the globe in ocular duction. *Invest Ophthalmol Vis Sci*. 2016;57(4):1826–1838. PMID: 27082297; PMCID: PMC4849549. doi:10.1167/iovs.15-18718
12. Wang X, Rumpel H, Lim WE, et al. Finite element analysis predicts large optic nerve head strains during horizontal eye movements. *Invest Ophthalmol Vis Sci*. 2016;57(6):2452–2462. PMID: 27149695. doi:10.1167/iovs.15-18986
13. Wang X, Beotra MR, Tun TA, et al. In Vivo 3-dimensional strain mapping confirms large optic nerve head deformations following horizontal eye movements. *Invest Ophthalmol Vis Sci*. 2016;57(13):5825–5833. PMID: 27802488. doi:10.1167/iovs.16-20560
14. Wang X, Fisher LK, Milea D, Jonas JB, Girard MJ. Predictions of optic nerve traction forces and peripapillary tissue stresses following horizontal eye movements. *Invest Ophthalmol Vis Sci*. 2017;58(4):2044–2053. PMID: 28384725. doi:10.1167/iovs.16-21319
15. Chang MY, Shin A, Park J, et al. Deformation of optic nerve head and peripapillary tissues by horizontal duction. *Am J Ophthalmol*. 2017;174:85–94. PMID: 27751810; PMCID: PMC5812679. doi:10.1016/j.ajo.2016.10.001
16. Suh SY, Le A, Shin A, Park J, Demer JL. Progressive deformation of the optic nerve head and peripapillary structures by graded horizontal duction. *Invest Ophthalmol Vis Sci*. 2017;58(12):5015–5021. PMID: 28973373; PMCID: PMC5627675. doi:10.1167/iovs.17-22596
17. Lee WJ, Kim YJ, Kim JH, et al. Changes in the optic nerve head induced by horizontal eye movements. *PLoS One*. 2018;13(9):e0204069. Erratum in: PLoS One. 2019 May 9;14(5):e0216861. PMID: 30226883; PMCID: PMC6143247. doi:10.1371/journal.pone.0204069
18. Demer JL, Clark RA, Suh SY, et al. Optic nerve traction during adduction in open angle glaucoma with normal versus elevated intraocular pressure. *Curr Eye Res*. 2020;45(2):199–210; PMID: 31453714; PMCID: PMC7398593. doi: 10.1080/02713683.2019.1660371
19. Clark RA, Suh SY, Caprioli J, et al. Adduction-induced strain on the optic nerve in primary open angle glaucoma at normal intraocular pressure. *Curr Eye Res*. 2021;46(4):568–578; PMID: 32911989; PMCID: PMC7947028. doi: 10.1080/02713683.2020.1817491
20. Ren R, Wang N, Li B, et al. Lamina cribrosa and peripapillary sclera histomorphometry in normal and advanced glaucomatous Chinese eyes with various axial length. *Invest Ophthalmol Vis Sci*. 2009;50(5):2175–2184. PMID: 19387083. doi:10.1167/iovs.07-1429
21. Jonas JB, Jonas SB, Jonas RA, Holsbach L, Panda-Jonas S. Histology of the parapapillary region in high myopia. *Am J Ophthalmol*. 2011;152(6):1021–1029. doi:10.1016/j.ajo.2011.05.006
22. Ohno-Matsui K, Akiba M, Moriyama M, et al. Imaging retrobulbar subarachnoid space around optic nerve by swept-source optical coherence tomography in eyes with pathologic myopia. *Invest Ophthalmol Vis Sci*. 2011;52:9644–9650. doi:10.1167/iovs.11-8597
23. Flitcroft DI, He M, Jonas JB, et al. IMI – defining and classifying myopia: a proposed set of standards for clinical and epidemiologic studies. *Invest Ophthalmol Vis Sci*. 2019;60(3):M20–M30. doi:10.1167/iovs.18-25957

24. Toranzo J, Cohen SY, Erginay A, Gaudric A. Peripapillary intrachoroidal cavitation in myopia. *Am J Ophthalmol*. 2005;140(4):731–732. doi:10.1016/j.ajo.2005.03.063
25. Freund KB, Mukkamala SK, Cooney MJ. Peripapillary choroidal thickening and cavitation. *Arch Ophthalmol*. 2011;129(8):1096–1097. PMID: 21825199. doi:10.1001/archophthalmol.2011.208
26. Spaide RF, Akiba M, Ohno-Matsui K. Evaluation of peripapillary intrachoroidal cavitation with swept source and enhanced depth imaging optical coherence tomography. *Retina*. 2012;32(6):1037–1044. doi:10.1097/IAE.0b013e318242b9c0
27. Kim TW, Kim M, Weinreb RN, et al. Optic disc change with incipient myopia of childhood. *Ophthalmology*. 2012;119(1):21–26. doi:10.1016/j.ophtha.2011.07.051
28. Tideman JW, Snabel MC, Tedja MS, et al. Association of axial length with risk of uncorrectable visual impairment for Europeans with myopia. *JAMA Ophthalmol*. 2016;134(12):1355–1363. PMID: 27768171. doi:10.1001/jamaophthalmol.2016.4009
29. Morgan IG, French AN, Ashby RS, et al. The epidemics of myopia: aetiology and prevention. *Prog Retin Eye Res*. 2018;62:134–149. doi:10.1016/j.preteyeres.2017.09.004
30. Grzybowski A, Kanclerz P, Tsubota K, et al. A review on the epidemiology of myopia in school children worldwide. *BMC Ophthalmol*. 2020;20(1):27. doi:10.1186/s12886-019-1220-0
31. Gomez-Salazar F, Campos-Romero A, Gomez-Campaña H, et al. Refractive errors among children, adolescents and adults attending eye clinics in Mexico. *Int J Ophthalmol*. 2017;10(5):796–802. PMID: 28546940; PMCID: PMC5437471. doi:10.18240/ijo.2017.05.23
32. Holden BA, Fricke TR, Wilson DA, et al. Global prevalence of myopia and high myopia and temporal trends from 2000 through 2050. *Ophthalmology*. 2016;123(5):1036–1042; PMID: 26875007. doi: 10.1016/j.ophtha.2016.01.006
33. Choudhury F, Meuer SM, Klein R, et al.; Chinese American Eye Study Group. Prevalence and characteristics of myopic degeneration in an adult Chinese American population: the Chinese American Eye Study. *Am J Ophthalmol*. 2018;187:34–42. doi:10.1016/j.ajo.2017.12.010
34. Fan H, Ma H, Gao R, et al. Associated factors for visibility and width of retrobulbar subarachnoid space on swept-source optical coherence tomography in high myopia. *Sci Rep*. 2016;6(1):36723. PMID: 27827444; PMCID: PMC5101481. doi:10.1038/srep36723
35. Anderson DR. Ultrastructure of human and monkey lamina cribrosa and optic nerve head. *Arch Ophthalmol*. 1969;82(6):800–814. PubMed: 4982225. doi:10.1001/archopht.1969.00990020792015
36. Wang X, Teoh CKG, Chan ASY, et al. Biomechanical properties of Bruch's membrane-choroid complex and their influence on optic nerve head biomechanics. *Invest Ophthalmol Vis Sci*. 2018;59(7):2808–2817. PMID: 30029276. doi:10.1167/iovs.17-22069
37. Chen JY, Le A, De Andrade LM, Goseki T, Demer JL. Compression of the choroid by horizontal duction. *Invest Ophthalmol Vis Sci*. 2019;60(13):4285–4291. doi:10.1167/iovs.19-27522
38. Le A, Shin A, Park J, Poukens V, Demer JL. Bilaminar Structure of the human optic nerve sheath. *Curr Eye Res*. 2020;45(7):864–872. PMID: 32155090; PMCID: PMC7286776. doi:10.1080/02713683.2020.1739314
39. Shin A, Park J, Le A, Poukens V, Demer JL. Bilaminar mechanics of the human optic nerve sheath. *Curr Eye Res*. 2020;45(7):854–863. PMID: 31821056; PMCID: PMC7286774. doi:10.1080/02713683.2019.1701689
40. Jonas JB, Holbach L, Panda-Jonas S. Peripapillary ring: histology and correlations. *Acta Ophthalmol*. 2014;92(4):e273–e279. PMID: 24373493. doi:10.1111/aos.12324
41. Wang X, Chang S, Grinband J, et al. Optic nerve tortuosity and displacements during horizontal eye movements in healthy and highly myopic subjects. Br J Ophthalmol. 2021:bjophthalmol-2021-318968. PMID: 34039559. doi:10.1136/bjophthalmol-2021-318968
42. Burgoyne CF, Downs JC, Bellezza AJ, Suh JK, Hart RT. The optic nerve head as a biomechanical structure: a new paradigm for understanding the role of IOP-related stress and strain in the pathophysiology of glaucomatous optic nerve head damage. *Prog Retin Eye Res*. 2005;24(1):39–73. PMID: 15555526. doi:10.1016/j.preteyeres.2004.06.001
43. Okuma S, Mizoue S, Ohashi Y. Visual field defects and changes in macular retinal ganglion cell complex thickness in eyes with intrachoroidal cavitation are similar to those in early glaucoma. *Clinical Ophthalmol*. 2016;10:1217–1222. doi:10.2147/OPTH.S102130
44. Marcus MW, de Vries MM, Junoy Montolio FG, Jansonius NM. Myopia as a risk factor for open-angle glaucoma: a systematic review and meta-analysis. *Ophthalmology*. 2011;118(10):1989–1994.e2. doi:10.1016/j.ophtha.2011.03.012
45. Demer JL, Clark RA, Suh SY, et al. Magnetic resonance imaging of optic nerve traction during adduction in primary open-angle glaucoma with normal intraocular pressure. *Invest Ophthalmol Vis Sci*. 2017;58(10):4114–4125. doi:10.1167/iovs.17-22093
46. Wang X, Rumpel H, Baskaran M, et al. Optic nerve tortuosity and globe proptosis in normal and glaucoma subjects. *J Glaucoma*. 2019;28(8):691–696. PMID: 31045951. doi:10.1097/IJG.0000000000001270